Ab initio study on the surface chemistry and nanotribological properties of passivated diamond surfaces

G. Zilibotti,[1,2] M. C. Righi,[1,*] and M. Ferrario[1,2]

[1]*Dipartimento di Fisica, INFM-CNR National Research Center on nanoStructures and bioSystems at Surfaces (S3), Università di Modena e Reggio Emilia, Via Campi 213/A, 41100 Modena, Italy*

[2]*Centre Européen de Calcul Atomique et Moléculaire (CECAM), Ecole Normale Supérieure, 46 Allée dItalie, 69007 Lyon, France*

Experimental findings indicate that the impressively low friction and wear of diamond in humid environments are determined by the surface passivation. In this paper, we investigate the relationship between the surface chemistry and the nanotribological properties of diamond surfaces. We consider the (2×1)-C(001) surface taking into account different terminations constituted of hydrogen, oxygen, and hydroxyl groups. We analyze the adsorbate geometry and the polarization of the surface bonds. We discuss the stability of the different surface terminations in different conditions, which account for the presence in the environment of H_2, O_2, and H_2O molecules in different concentrations and we present the surface phase diagram. Finally, we report the calculated adhesion energy between the passivated surfaces and analyze its variation as a function both of the surface separation and of the surface relative lateral position. In this way, we provide information on the effect of the different adsorbates on the interaction between diamond surfaces and on the magnitude and anisotropy of friction forces.

I. INTRODUCTION

Carbon-based films, which range from diamond in single crystal or polycrystalline form, to amorphous films with a mixture of sp^2 and sp^3 bondings—known as diamondlike coatings (DLC)—present outstanding tribological properties. Coefficients of friction (COF) are below 0.05, which is as slippery as ice, and wear rates are extremely low. Due to these properties, diamond films are used as coatings for cutting tools, biological implants, bearings, and more recently as structural materials for microelectromechanical systems (MEMS). DLC coatings are employed in many applications that range from hard disks to aerospace and automotive components.[1] The capability of showing very low friction and high wear resistance without any oil or chemical additive makes the carbon-based films advantageous for the environment. Thus, diamond and diamondlike coatings seem to be the most promising materials for the present and future tribology.

However, the widespread use of carbon films has been hindered, in particular at the nanoscale, by the difficulty to reproduce and control the tribological properties of these materials in different environments. It is well known that the COF of diamond can increase to 2/3 orders of magnitude in vacuum or in dry conditions[2–4] with respect to air, with wear becoming severe. In the same way, the tribological properties of DLC films highly depend on the H contents in the film structure[5] and on the relative humidity of the ambient atmosphere.[6] These effects, along with friction dependence on surface structure orientation, deeply affect the functionality of microscopic objects where the surface/volume ratio is high. The most widely used experiments for investigating the microscopic mechanisms that influence the tribological properties of nanoscale materials are those based on the atomic force microscope (AFM) which allows to measure the forces acting against the motion of a tip scanning, as a single as-

perity, the underlying surface. From a theoretical point of view, it is possible to derive information on these forces by calculating the potential-energy surface (PES) of a sliding interface. The PES can be constructed by calculating the interaction energy of the two surfaces in contact for different relative lateral positions. The slope of the PES profile along a given direction corresponds to the force acting against sliding along that direction. Another quantity that influences the tribological properties of nanoscale objects which can be derived by calculations is the adhesion energy between the two surfaces in contact. This quantity can be compared with the work of separation measured in the experiments through the pull off force, i.e., the force required to pull the tip out of contact with the surface.

In this work, we performed *ab initio* calculations to get insight into the tribological properties of diamond interfaces (however, most of the considerations may hold for DLC as well) with a particular focus on the effects of adsorbates such as hydrogen, oxygen, and hydroxyl groups. The *ab initio* calculations can accurately describe the surface chemistry, which has been experimentally demonstrated to play an important role in influencing the tribological properties of carbon-based films.

Different experimental[4,5,7] and theoretical[8–10] studies have highlighted the beneficial effect of hydrogen termination on the tribological properties of carbon-based materials, while the interaction of diamond surfaces saturated by hydroxyl groups or oxygen has been much less investigated, in particular, from a theoretical point of view. However, this is rather an important issue since it is known that the interaction of water vapor with clean diamond surfaces results in the dissociative adsorption of water.[11,12] Moreover, a recent work demonstrates that the origin of ultralow friction and wear in diamond is the surface passivation occurring during sliding in environments containing gaseous species, in particular, water vapor. The surface spectroscopic analysis after

the tribological test in humid air revealed the presence of C-H and C-O bonds.[13] A similar effect has been invoked to explain the drop in friction coefficient of hydrogen-free DLC films upon introduction into the test chamber of moist air.[6] Indeed water (or hydroxyl-containing molecules such as glycerol[14,15]) is attracting interest as a possible environmental-friendly lubricant for carbon-based materials.[16,17]

We considered the (001) surface of diamond. This surface is of interest because of the advances in chemical vapor deposition (CVD) growth process to obtain atomically smooth thin films.[18] It presents a (2×1) dimer reconstruction which can give rise to friction anisotropy, as it will be discussed. Starting from the (2×1)-C(001) phase, we studied the most likely surface terminations in (humid) air: hydroxylation, H_2O termination, hydrogenation, and oxygenation. We performed the surface structural relaxation and energy optimization within the density-functional theory (DFT) approach. Preliminary calculations on the diamond bulk properties allowed us to evaluate the accuracy of different generalized gradient approximations (GGA) for the exchange-correlation functional and to select the most suitable one. The results we obtained for the optimized adsorbate geometry can be compared with those present in the literature which were derived within the local-density approximation (LDA). As a further contribution to the study of the surface chemistry of the passivated diamond surfaces, we analyzed the stability of the different surface terminations in different environments and we constructed the $T=0$ phase diagram of the C(001) surface as a function of the hydrogen and oxygen chemical potentials. In addition, through the Löwdin population analysis,[19] we calculated the polarization of the surface bonds for the different terminations. Indeed, we found that the presence of surface dipoles plays a role on the interaction between the passivated diamond surfaces. In order to get insight into the tribological properties of diamond, we calculated the interaction energy between two surfaces in contact both for different separation distances and for different lateral positions, i.e., constructing the perpendicular PES (P-PES) and a lateral PES (L-PES) of the interface, respectively. The former provides information on the nature and the strength of the surface interaction. The latter indicates how much and in which way the interaction energy varies as one surface is moved relative to the other one, thus providing information on the magnitude of friction forces and on friction anisotropy. The interface calculations were performed for the different surface terminations that we have considered.

II. METHOD

We performed plane-wave/pseudopotential first-principles calculations[20] based on DFT. We selected the approximation for the exchange-correlation functional (xc) by performing test calculations on the structural and electronic properties of *bulk* diamond. We compared LDA and GGA in two different parametrizations, namely, PW91 (Ref. [21]) and PBE.[22] The results are reported in Table I. We can see that the values obtained within the PBE approximation are in closer agree-

TABLE I. The accuracy of different approximations for the exchange-correlation functional is tested in reproducing structural and electronic parameters of bulk diamond; namely, the equilibrium lattice constant a, the bulk modulus B, the energy gap E_{gap}, and the energy gap at the **k**-point Γ ($E_{gap,\Gamma}$). The PBE values are in closer agreement with the experiments.

	a (Å)	B (GPa)	E_{gap} (eV)	$E_{gap,\Gamma}$ (eV)
LDA	3.527	460	3.56	5.51
PBE	3.576	428	4.15	5.60
PW91	3.577	427	4.11	5.57
Expt.[a]	3.57	443	5.3	6.0

[a]Reference [23].

ment with experiments; thus we adopted this approximation in the following calculations of diamond surfaces and interfaces. The calculations were performed employing ultrasoft pseudopotential generated with the same xc approximation used in self-consistent calculations. After test calculations, the cut-off energy for plane-wave expansion was chosen as 30 Ry.

The *surfaces* were modeled using periodic supercells with a (2×1) in-plane size. A large amplitude for the vertical c axis was chosen in view of interface calculations where two slabs were included within the same supercell. We used c $=29$ Å to simulate two surfaces in contact and $c=50$ Å to simulate two surfaces farther apart than the equilibrium distance up to the noninteracting situation, where the two slabs are separated by 15 Å of vacuum from both sides. The slab bottom layer was passivated with H atoms (two for each C atom) in all the surfaces except for the oxygen-terminated ones which were modeled with symmetric slabs to avoid spurious electrostatic interactions induced by the periodic boundary conditions. Tests on the slab thickness revealed that nine layers of carbon were sufficient to reproduce the effect of a semi-infinite bulk. We have, in fact, optimized the geometry of the C(001) surface considering both a slab of nine layers and a slab of 13 layers. We found that the geometrical parameters characterizing the (2×1)-dimer reconstruction did not significantly differ in the two cases and that the surface relaxation did not penetrate further than the first few layers of the slabs. Furthermore, the difference in surface formation energy we obtained in the two calculations was of about 2 meV. These results along with the gain of computational resources motivate our choice of considering a nine layer slab thickness. We tested the accuracy of the total energy with respect to the number of **k** points of the Monkhorst Pack grid[24] adopted to sample the Brillouin zone (BZ), and we found that the results converged with a $(5 \times 10 \times 1)$ grid.[25]

As anticipated in Sec. I, we studied the C(001) surface taking into consideration different terminations which can originate upon exposure to air (which contains N_2, O_2, and H_2O molecules) or upon H treatment. The considered passivated surfaces are (A) the fully hydroxylated surface "OH-C(001)" terminating with a layer of -OH groups, (B) the termination obtained by the dissociative adsorption of a wa-

ter molecule, the "H_2O-C(001)" surface containing both CH and COH bonds; (*C*) the fully hydrogenated "H-C(001)" surface terminating with a complete monolayer of hydrogen atoms; and (*D*) the fully oxygenated surface "O-C(001)" terminating with a complete monolayer of oxygen atoms. For the surface terminations where different adsorbate arrangements were possible, we identified the most likely adsorption configuration by comparing the total energies. Each surface structure was optimized allowing all the atoms of the slab to move until each force component became smaller than 10^{-3} Ry/a.u. and the system total energy varied less than 10^{-4} Ry. As a result, we obtained the parameters characterizing the adsorbate geometry and their adsorption energies.

Due to the different electronegativity of the C (2.5), H (2.2) and O (3.5) elements, the C-H and O-H bonds on the surface have a polarization which affects both the adsorbate-adsorbate interaction within the same surface and the interaction between two surfaces in contact. We performed the Löwdin population analysis in order to identify the charge displacement occurring on polar bonds. This is done by projecting the electronic wave functions on a localized basis set. The noncompleteness of the set usually results in the lack of a small portion of the total charge, i.e., the spilling parameter. In our calculations, we obtained a small value for the spilling parameter, corresponding to 0.5% of the total charge.

We concluded our analysis on the passivated diamond surfaces by analyzing the surface stability in different conditions, i.e., taking into consideration different molecular precursors. In particular, we considered H_2, H_2O, and O_2 molecules. The isolated molecules were modeled adopting a cubic supercell of about 20 Å edge, using the Γ point only for BZ sampling. The optimized molecular structures are in good agreement with experiments. The calculated values for the bond lengths are $d_{H\text{-}H}=0.75$ Å ($d_{H\text{-}H}^{exp}=0.75$ Å), $d_{H\text{-}O}=0.97$ Å ($d_{H\text{-}O}^{exp}=0.96$ Å), and $d_{O\text{-}O}=1.23$ Å ($d_{O\text{-}O}^{exp}=1.21$ Å). For the angle in the water molecule, we obtained $\theta=104.3°$ ($\theta^{exp}=105°$). By comparing the energy of the water molecule with the energy of its constituent ($H_2+\frac{1}{2}O_2$), we calculated the water formation energy $\Delta E=-2.97$ eV (to be compared with $\Delta E=-2.53$ eV obtained from the experimental value for the standard enthalpy of formation $\Delta H^{exp}=-2.51$ eV for water in the gas phase[26]).

As a next stage in our investigation, we considered *interfaces* between two diamond surfaces in order to get insight into the tribological properties of carbon-based materials. Here we call "interface" a system consisting of two parallel surfaces facing each other modeled by two commensurate mirror slabs separated by an initial distance Dz_0 of 1.5 Å. We constructed the *lateral PES* experienced by a sliding interface, taking into account different relative lateral positions of the two surfaces. The position of the upper surface with respect to the underlying one was chosen on a homogeneous grid of points separated by linear spaces $\Delta x=\Delta y=1.26$ Å, as illustrated in Fig. 1. Each point of the grid indicates the position of the center of the dimer belonging to the (2×1) cell of the upper surface (not shown) within the (2×1) cell of the underlying surface. The grid points are labeled by T capital letters, indicating that they belong to a "top sliding channel" where the superimposition between the dimers of the two surfaces is higher, and by H capital letters, indicating
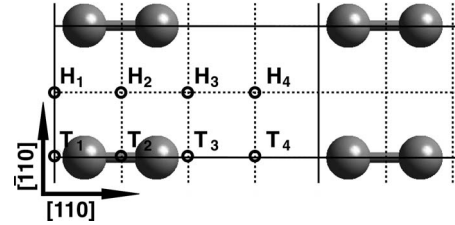

FIG. 1. Top view of the (2×1)-C(001) surface. Only the atoms belonging to the topmost carbon layer are shown in their optimized configuration. The homogeneous grid used to calculate the PES of two commensurate surfaces in relative motion is represented by the dashed lines. Each grid point indicates the location of the center of the dimer belonging to the (2×1) cell of the upper surface (not shown) within the unit cell of the underlying surface. The grid points are labeled according to the convention explained in the text.

that they belong to a "hollow sliding channel" where the superimposition between the dimers of the two surfaces is lower. For each grid point, we performed a structural relaxation of the system under the following constraints. We fixed the bottom three layers of the lower slab and the (x,y) degrees of freedom of the atoms belonging to the three topmost layers of the upper slab. In this way, during the relaxation the distance between the two surfaces could reach its equilibrium value Dz_{eq}. For each relative lateral position (x,y), we calculated the interaction energy $V(x,y,z_{eq})$ of the two surfaces, as $V=E_{12}^{tot}-E_{1+2}^{tot}$, where E_{12}^{tot} is the total energy of two interacting surfaces and E_{1+2}^{tot} is the total energy of two noninteracting surfaces, i.e., of two surfaces separated by 15 Å of vacuum. According to this definition, negative values of V indicate an adhesive interaction between the two surfaces. From the calculated value of V it is possible to estimate the work of separation; a quantity which can be measured by experiments defined as the energy per unit area required to separate the surfaces from contact to infinity,[27]

$$W_{sep} = \gamma_1 + \gamma_2 - \gamma_{12} = -V/A, \qquad (1)$$

where γ_{12} is the interfacial energy, γ_1 and γ_2 are the energies of the two isolated surfaces, and A is the interface area (in our case the in-plane surface of the supercell).

In order to better understand the physical origin of the interactions between the two surfaces in contact, we calculated the *perpendicular PES*, i.e., the variation in the interaction energy as a function of the surfaces distance $V([x,y]_{min},z)$. The P-PES was calculated considering the surfaces at the lateral position ($[x,y]_{min}$) corresponding to the minimum of the L-PES. For each vertical distance, a relaxation of the system was achieved allowing all the atoms free to move except for those belonging to the three bottom layers of both the slabs.

III. RESULTS

A. Optimized adsorption structure and energetics of passivated C(001) surfaces

The (2×1) reconstruction of the C(001) surface presents carbon dimers along the [110] direction. The topmost surface
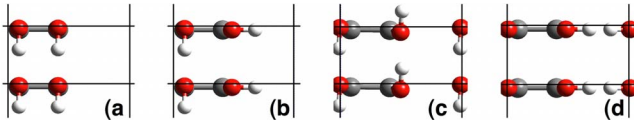
FIG. 2. (Color online) Top view of the initial configurations considered for constructing the hydroxylated surface termination. They are characterized by different positions of the OH groups with respect to the carbon dimer. After the structural relaxation, the adsorption geometry of panel (c) turned out to be the most favorable one.

layer of the optimized surface is shown in Fig. 1. The calculated dimer length (1.35 Å) is shorter than the carbon bond length in bulk diamond (1.55 Å), indicating the existence of a double C=C bond within the dimer. These results are in agreement with previous theoretical studies.[28] Starting from this configuration, we considered the passivated surfaces described in the following.

1. OH-C(001)

We constructed the fully hydroxylated surface taking into account all the dispositions for the OH groups that are possible within the (2×1) cell; they are represented in Fig. 2. We did not consider adsorption configurations with a larger periodicity than the (2×1) one because the main purpose of the paper is to study the effect of adsorbates on the adhesion and friction properties of diamond interfaces. We think that the adsorbates arrangement on the surface can influence the friction anisotropy and, only to a minor extent, the friction intensity. During the relaxation process, the OH group that is oriented perpendicularly to the carbon dimer in Fig. 2(b) moved along the cell diagonal with the H atom pointing to the O atom of the other hydroxyl group contained in the cell. The surface configuration of Fig. 2(d) spontaneously reached the configuration of Fig. 2(c). These structural optimizations are most likely dictated by the tendency to form hydrogen bonds between OH groups. The Lödwin population analysis revealed, in fact, the presence of a charge displacement along the hydroxyl group $O^{\delta-}$-$H^{\delta+}$, with $\delta- = 0.5e$ and $\delta+ = 0.4e$. The configurations having lowest energy turned out to be those presenting the OH groups oriented perpendicularly to the carbon dimer [Figs. 2(a) and 2(c)], where OH···OH chains connected by hydrogen bonds can be established along the $[\bar{1}10]$ direction. The distance of 2.53 Å between the oxygen atoms belonging to different OH groups along this direction is in fact compatible with the presence of a hydrogen bond. The lowest energy is obtained by an antiparallel disposition of the OH dipoles [Fig. 2(c)]. The optimized surface geometry for this configuration is represented in Fig. 3(a), where the most relevant geometric parameters and the charge of the atoms belonging to polar bonds are reported.

2. H₂O-C(001)

We considered a surface termination resulting from the dissociative adsorption of one H_2O molecule per (2×1) cell. It consists of a H atom and a OH group attached to the carbon atoms of the dimer. The energy barrier for H_2O dis-

sociation estimated by Okamoto[29] on the basis of hybrid molecular orbitals-DFT calculations is of 1.12 eV, while the energy barrier for water dissociation on the C(111) surface was estimated of about 0.12 eV by Qi *et al.*[30] on the basis of DFT calculations. We identified the most stable adsorption geometry for the hydroxyl group by comparing the energy of three configurations differing for the orientation of the OH bonds: we considered the [110], $[\bar{1}10]$, and [100] directions. As it happened for the fully hydroxylated surface, we found that the most stable structure is that presenting the hydroxyl group oriented along the $[\bar{1}10]$ direction, that is, perpendicularly to the carbon dimer. The optimized structure of this configuration is shown in Fig. 3(b). The Lödwin population analysis revealed that the OH group presents the same polarization as in the fully hydroxylated surface and that the CH bond also is a polar bond $C^{\delta-}$-$H^{\delta+}$, with $\delta- = 0.15e$ and $\delta+ = 0.2e$.

3. H-C(001)

The hydrogen termination is often observed in diamond (or DLC) films exposed to hydrogen flows. The monohydride configuration is known to be the most stable configuration for the fully hydrogenated C(001) surface.[31] The optimized structure is reported in Fig. 3(c). As done for the other structures, we calculated the Lödwin charges and we found that each CH bond is polar with a displacement of $0.2e$ from the H to the C atom.

The hydrogenated diamond surface is of particular interest because a recent paper which appeared on Science demonstrates that this surface presents a high conductivity when exposed to humid air.[32] The authors attributed the surface conductivity to the difference in the Fermi level of diamond compared to the Fermi level of the adsorbed water film which enables electrons to flow from the diamond to the water. This leads to the formation of positive holes in diamond that conducts electricity. These findings can have a considerable impact on the frictional behavior of hydrogenated diamond surfaces. First, because the presence of a conductive substrate can offer an additional channel for energy dissipation besides the excitation of phonons, giving rise to an electronic contribution to friction. Second, because the otherwise hydrophobic diamond would attract a layer of water. An electrostatic attraction develops between the positively charged diamond surface and the compensating anions in the aqueous phase. This attraction has been detected by the authors by measuring a decrease in the contact angle between hydrogenated diamond and water at low pH. The capability of the surface to "self-lubricate" by attracting water molecules may positively affect its friction properties. We have, in fact, found that the friction forces between diamond surfaces can increase by some orders of magnitude if carbon dangling bonds are present at the interface.[33] The existence of a layer of water molecules covering the surface may guarantee a reservoir of chemical species which can continuously saturate the carbon dangling bonds that originate at the sliding interface.

4. O-C(001)

The last surface termination we considered is the fully oxygenation. The interaction of water vapor present in the air
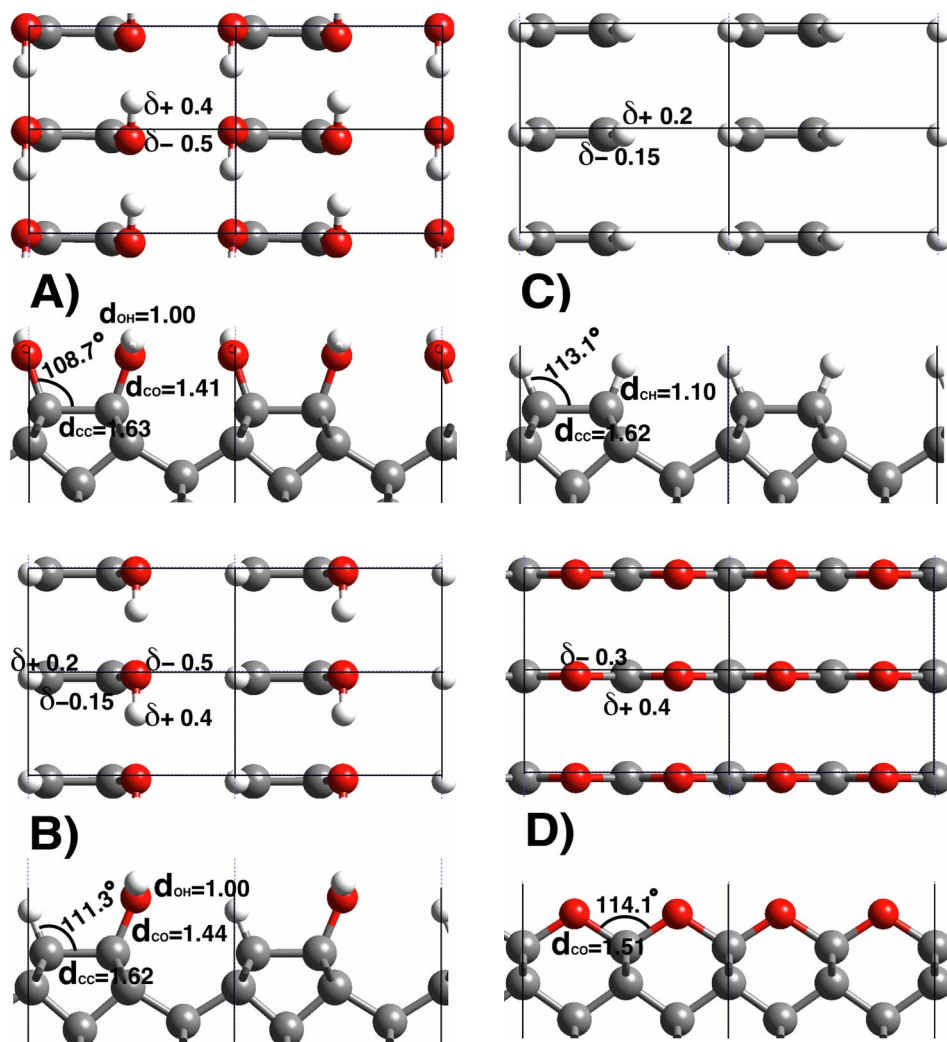
FIG. 3. (Color online) Top and lateral views of the optimized structure of the passivated diamond surfaces we have considered, namely, hydroxylated (*A*), H_2O-terminated (*B*), hydrogenated (*C*), and oxygenated (*D*) surfaces. In the upper part of each panel, representing the surface top view, the excess (lack) of charge calculated by means of the Lödwin population analysis is reported on each atom belonging to a polar bond; while the main geometrical parameters characterizing the adsorbate configuration are reported in the bottom part of each panel, representing the surfaces lateral view.

with clean diamond (001) mostly produces C-H and C-OH bonds, as indicated by the high-resolution electron-energy-loss spectroscopy (HREELS) measurements of Gao *et al.*[12] However, we considered that it is also interesting to study oxygenated diamond surfaces because C-O- and C=O-terminated domains may originate from further decomposition processes from the adsorbed hydroxyl fragments. The activation energy for such processes could come from the mechanical energy supplied during the tribological process. Indeed the spectroscopic analysis performed by Konicek *et al.*[13] revealed an increase of C-O and C=O bondings after the tribological test. We modeled oxygenated surfaces by means of symmetric slabs, as explained in Sec. II. We took into account two different adsorption configurations for the oxygen atoms: the *ether* and the *ketone* configurations.[34] In the former case, each oxygen atom occupies a bridge position between the two carbon atoms originally bonded in the dimer which is now broken and a chain of C-O-C bonds is established along the [110] direction. In the latter case, the oxygen atom adsorbs on top of each carbon atom establishing a double C=O bond perpendicular to the surface. Also in this case, the original carbon dimer disappears and the surface acquires a (1×1) periodicity. The comparison between the total energies of the two systems revealed that the ether adsorption configuration is more

stable than the ketone one by 0.35 eV per oxygen atom. Previous LDA calculations evaluated an energy difference of 0.6 eV (Ref. 34) and of 0.5 eV (Ref. 35) per oxygen atom. Due to the higher stability, the ether configuration will be considered in the following analysis on oxidized diamond interfaces. The Lödwin population analysis revealed that the ether termination presents a strong polarization. For the $C^{\delta+}$-$O^{\delta-}$ polar bonds we found $\delta+ = 0.2e$ and $\delta- = 0.3e$.

We conclude this part of the paper devoted to the study of the passivated diamond surfaces by calculating the surface formation energy ΔE in different conditions and by discussing the relative stability of the different surface terminations. The formation energy can be obtained as the difference between the energy of the reactants, which in our case correspond to the clean C(001) surface plus precursor molecules, and the products corresponding to the passivated surfaces plus what is left of the molecular precursors. We considered H_2, O_2, and H_2O precursors. We identified four groups of molecular precursors which can give rise to all the surface terminations we have considered. They are reported in the first line of Table II. We can see that in quite all the cases the surface passivation is an exothermic process with an associated enthalpy of few eV per (2×1) cell. The surface passivation process turns out to be most energetically favorable when it involves H_2 and O_2 molecules. The mean energy

TABLE II. Energies ΔE [eV/(2×1) cell] of different passivation processes for the C(001) surface. We have considered four groups of reactants reported in the first row. As products, we considered the passivated surfaces OH-C(001) (A), H_2O-C(001) (B), H-C(001) (C), and O-C(001) (D) plus what of the precursors is left by the dissociative adsorption. The same analysis has been done for the interfaces, considering a double number of reactant molecules and all the possible couples of passivated surfaces. In this case, only the energy corresponding to the most stable product has been reported in the last row.

C(001)+H_2+O_2		C(001)+H_2+$2H_2O$		C(001)+O_2+H_2O		C(001)+$2H_2O$	
Products	ΔE	Products	ΔE	Products	ΔE	Products	ΔE
A	−8.4	$A+2H_2$	−2.5	$A+\frac{1}{2}O_2$	−5.5	$A+H_2$	−2.5
$B+\frac{1}{2}O_2$	−6.7	$B+H_2+H_2O$	−3.7	$B+O_2$	−3.7	$B+H_2O$	−3.7
$C+O_2$	−4.5	$C+2H_2O$	−4.4	$C+\frac{3}{2}O_2$	−1.5	$C+\frac{1}{2}O_2+H_2O$	−1.5
$D+H_2$	−5.8	$D+3H_2$	+0.1	$D+H_2O$	−5.8	$D+2H_2$	+0.1
$A//A$	−16.9	$C//C+4H_2O$	−8.9	$D//D+2H_2O$	−11.6	$B//B+2H_2O$	−7.3

gain is—in fact—minimum for the reactions reported in column four, where the molecular precursors are water molecules, and maximum in column one, where only molecular oxygen and hydrogen are involved. Of course the occurrence of one kind of reaction rather than another one is also dictated by the magnitude of the energy barrier associated to the molecule dissociative adsorption. Experimental observations indicate that water dissociatively adsorbs on clean diamond surfaces.[11,12]

As can be seen from Table II, the relative stability of the different surface terminations depends on the gas molecules from which the adsorbed oxygen and hydrogen come. The energy of each surface depends, in fact, on the chemical potential of the constituting species. A more complete picture of the stability can be obtained by considering the surface formation energy as a function of the chemical potentials. If we refer the energy of a surface to the energy of the clean surface, we can write

$$\Delta E_f = \Delta E_{tot} - n_H \mu_H - n_O \mu_O, \qquad (2)$$

where ΔE_{tot} is the energy difference between the passivated surface and the clean C(001) surface, n_i is the number of atoms of specie i adsorbed on the surface, and μ_i is their chemical potential. Since we are considering a gaseous environment which can contain either molecular hydrogen (oxygen) or water vapor, we can assume as upper bound for μ_H (μ_O) half of the energy of the H_2 (O_2) molecule and rewrite Eq. (2) as

$$\Delta E_f = \Delta E_{tot} - n_H \left(\frac{1}{2}\mu_{H_2} + \Delta\mu_H \right) - n_O \left(\frac{1}{2}\mu_{O_2} + \Delta\mu_O \right), \qquad (3)$$

where $\frac{\Delta E}{2} \leq \Delta\mu_H \leq 0$ and $\Delta E \leq \Delta\mu_O \leq 0$. The lower bounds of the chemical potentials are arbitrarily chosen assigning a fraction of the water formation energy ΔE to hydrogen and its double to oxygen. The condition $\Delta\mu_H = 0$ indicates hydrogen rich conditions, while $\Delta\mu_H = \frac{\Delta E}{2}$ indicates hydrogen poor conditions. According to these definitions, we constructed the $T=0$ phase diagram of the C(001) surface, which is represented in Fig. 4. In the picture, each point indicates through a different color the surface termination which is the most

stable for given values (μ_H, μ_O) of the hydrogen and oxygen chemical potentials. To construct the phase diagram, we compared the surface energy [Eq. (2)] of the four surface terminations of Fig. 3 and the clean surface. By looking at the results represented in Fig. 4 we can derive the following conclusions. (i) The clean diamond surface is never favored: passivated surfaces are more stable than the clean (2×1)-C(001) for all the considered values of the hydrogen and oxygen chemical potentials. (ii) In the presence of both molecular hydrogen and molecular oxygen, the most favorable surface termination is the fully hydroxylated surface (A), which is the condition of column one of Table II. By decreasing the oxygen content in the environment, as in the case of reactants of columns two and four of Table II, the most stable phases turned out to be the H_2O-terminated surface (B) and, in extremely hydrogen rich conditions, the fully hydrogenated surface (C). On the contrary, in oxygen rich conditions (column three of Table II) the oxygenated surface (D) is the most stable termination. (iii) The line superim-
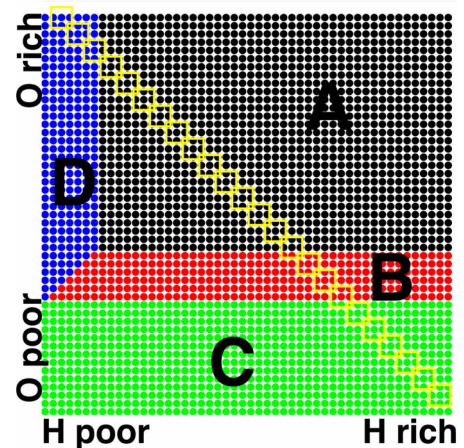

FIG. 4. (Color online) Phase diagram of the (001) surface of diamond. The different domains represent the most stable surface termination for the given values of oxygen and hydrogen chemical potentials. The latter can assume a wide range of values, taking into account in this way the presence of different molecular precursors, which ranges from H_2 (O_2) to water. The line indicates the condition $2\mu_H + \mu_O = \mu_{H_2O}$.

TABLE III. Adhesion energies for (2×1) cell (V^{min}) and equilibrium distance between the surfaces (Dz_{eq}) obtained for each interface at the grid point corresponding to the minimum of L-PES (min). The values of the maximum corrugation of each L-PES (ΔV^{max}) are calculated as the difference between the minimum and the maximum values of the adhesion energy. The grid points corresponding to the maxima of the L-PES are also reported (max).

	V^{min} (meV)	Dz_{eq} (Å)	Min	ΔV^{max} (meV)	Max
OH-C(001)	−10	2.9	H_3	10	T_2
H2O-C(001)	−12	2.5	H_3	8	T_3
H-C(001)	−8	3.0	T_2	4	H_3
O-C(001)	−5	3.6	T_3	2	H_2

posed on the phase diagram represents the condition $2\mu_H + \mu_O = \mu_{H_2O}$, indicating that the adsorbates are in thermodynamic equilibrium with water vapor. Since the line passes thorough all the four domains, we can conclude that all the surface terminations we have considered can be formed in a gaseous environment containing water vapor.

B. Adhesion and friction of passivated diamond surfaces

In order to get insight into the effect of the adsorbates on the tribological properties of diamond, we considered four interfaces constituted each by two specular surfaces. We expect that the interfaces containing two different surface terminations present an intermediate behavior with respect to the homogeneous interfaces considered here. Furthermore, homogeneous interfaces are always energetically more favorable than mixed interfaces, as can be seen from the last row of Table II, where the formation energy of the most stable interface is reported for each group of precursors. The interface formation energy is calculated as the sum of the formation energies of the two facing surfaces. The interaction energy between the two surfaces at equilibrium distance, which is of the order of few meV/(2×1) cell as it will be shown in the following, does not alter this conclusion on the interface relative stability.

We identified the equilibrium interface configuration by allowing the two mirror slabs, initially positioned at 1.5 Å vertical distance, to relax according to the constraints described in Sec. II. For each kind of termination we observed that during the relaxation process the two surfaces repulsed each other until the top slab—free to move along the z direction—reached an equilibrium distance Dz_{eq} far apart from the underlying surface: Dz_{eq} ranged, in fact, from 2.5 Å for the H_2O-terminated interface to 3.6 Å for the oxygenated interface. This behavior is most likely dictated by the presence of a layer of polar bonds on each surface, as it has been described in Sec. III A 4. In column one of Table III, the interaction energy (V) of the two facing surfaces at the equilibrium distance (Dz_{eq}) is reported. Dz_{eq} is in column two. The reported values of V refer to the surface lateral position corresponding to the L-PES absolute minimum, which is indicated in the third column of the table. It is interesting to observe that in the case of interfaces containing OH groups, the L-PES absolute minima are located within the hollow channel; while for hydrogenated and oxygenated

interfaces they reside within the top channel. This fact can be explained by considering the different spatial orientation of the polar bonds. The OH groups are parallel to the surfaces while the CH and CO bonds are oriented perpendicularly to the surfaces. As can be seen in Fig. 5, which contains a lateral view of the optimized interfaces, the interface configuration corresponding to the L-PES minima coincides to the relative position of the two surfaces where the electrostatic interaction between the adsorbates of opposite charge is maximized. The small values of the surface interaction energies, which are of the order of few meV/(2×1) cell (column one of Table III), and the large surface separations (column two) rule out the presence of any chemical interaction between the passivated diamond surfaces. The surface adhesion indicated by the negative sign of the interaction energy V is thus determined by dipole-dipole interactions. It is well known that DFT calculations based on LDA or equally on GGA, where the exchange-correlation energy is a functional of the local electronic density, are not able to accurately describe nonlocal interactions, such as the van der Waals interaction; thus the values reported in Table III are most likely underestimated. However, the trends which highlight differences in the effect of the different adsorbates can be considered reliable. Furthermore, we can observe that the description offered by the present calculations is not too far from reality as revealed by comparison with the experiments. The work of separation we estimate for the hydrogenated interface of 0.010 J/m^2 is in agreement with the work of separation of 0.0102 ± 0.004 J/m^2 measured experimentally for a diamond-covered tip on a hydrogenated diamond surface.[7]

Differences in the interaction between passivated surfaces can be appreciated by analyzing the variation of V as a function of the distance between the surfaces $V(z)$. In Fig. 6 we report the perpendicular PESs calculated for the four considered interfaces according to the methodology described in Sec. II. For a better comparison, we report in the picture the curves obtained at the same relative lateral position. We chose the H_3 grid point which corresponds to the L-PES minimum for the interfaces containing hydroxyl groups. We can see that all four curves present the typical features of the physisorption interaction. They are, in fact, characterized by a shallow minimum originating from the combination of a highly repulsive interaction at short range and a weak attraction at long range. The similar behavior of the black, red
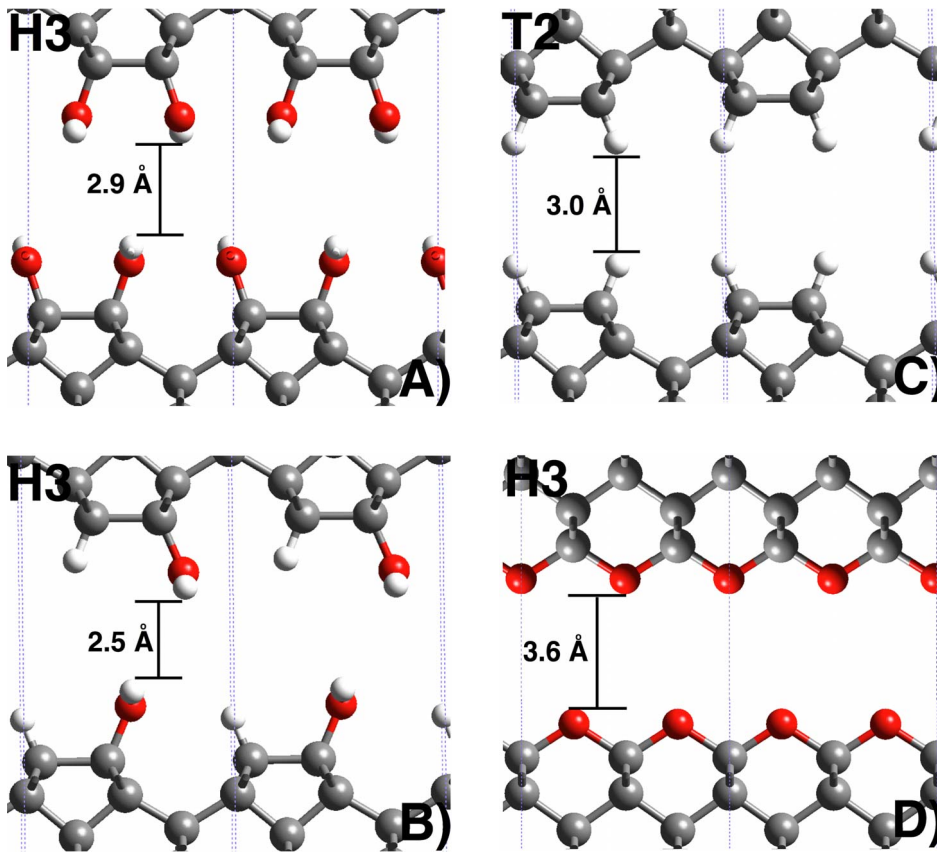
FIG. 5. (Color online) Lateral view of the relaxed interface configurations obtained for hydroxilated (*A*), H$_2$O-terminated (*B*), hydrogenated (*C*), and oxygenated (*D*) facing surfaces. The snapshots are relative to the lateral position of the two surfaces corresponding to the absolute minimum of the L-PESs. The label of the corresponding grid point is reported in each picture. The equilibrium distance between the two surfaces is also indicated.

(gray), and blue (dark gray) curves at the short distances, where they are almost parallel and steeper than the green (light gray) curve representing the hydrogenated interface, indicate that the repulsive energy in these interfaces is dominated by the interaction between the oxygen atoms, which possess higher ionicity than the other atoms involved in polar bonds. This fact explains also the shift toward higher values of Dz observed for the position of the minimum of the P-PES calculated for the oxygenated interface (blue-dark gray curve). While the shift toward shorter values of Dz observed for the position of the minimum of the P-PES for the H$_2$O-C(001) interface is most likely due to the formation of hydrogen bonds across the interface between the CH group of one surface and the OH group of the other one. The adsorbate distance and the bond directions can allow, in fact, the formation of hydrogen bonds across the H$_2$O-C(001) interface. We can conclude this analysis on the effect of the adsorbates on the interaction between diamond surfaces by observing that the main effect of the adsorbates is to prevent the formation of covalent C-C bond across the diamond interfaces. The repulsive interaction detected at the short distances causes the surfaces to move far apart where the energy modulations due to the lateral movement of one surface with respect to the other are of small amplitude, with benefits for friction.

The effect of the different adsorbates on the frictional properties of the passivated diamond surfaces can be well understood by observing the L-PESs obtained for the different interfaces, which are reported in Fig. 7. The plots are obtained thorough a bicubic interpolation of the adhesion energy calculated at the grid points used to sample the

(2×1) unit cell (Fig. 1). Different colors represent different values of the adhesion energy relative to its absolute minimum, that is, the potential corrugation (ΔV). The maximum value of ΔV calculated for the different passivated interfaces is reported in Table III. As explained in Sec. I, the potential corrugation governs the frictional behavior of the system. We can observe that the higher the adhesion, the higher is the potential corrugation. The hydrogenated interfaces and, in particular, the oxygenated ones present very smooth PESs. In these cases, the two surfaces at the sliding interface stand far
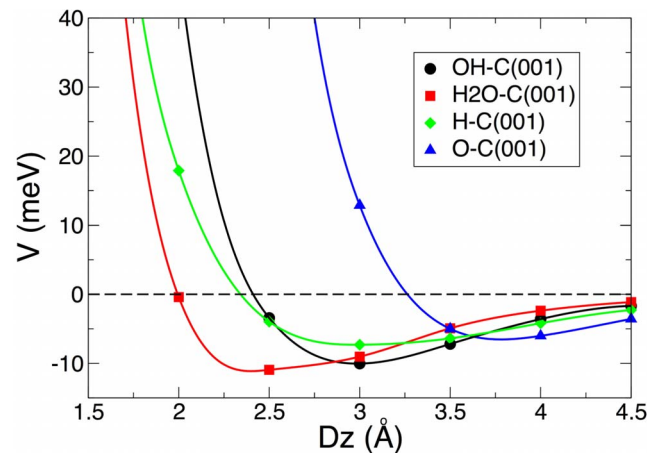

FIG. 6. (Color online) Perpendicular PESs describing the variation in the interface energy V as a function of the distance between the surfaces. Dz indicates the distance along the z direction calculated between the surfaces after the relaxation process, which was executed under the constraints described in the text.
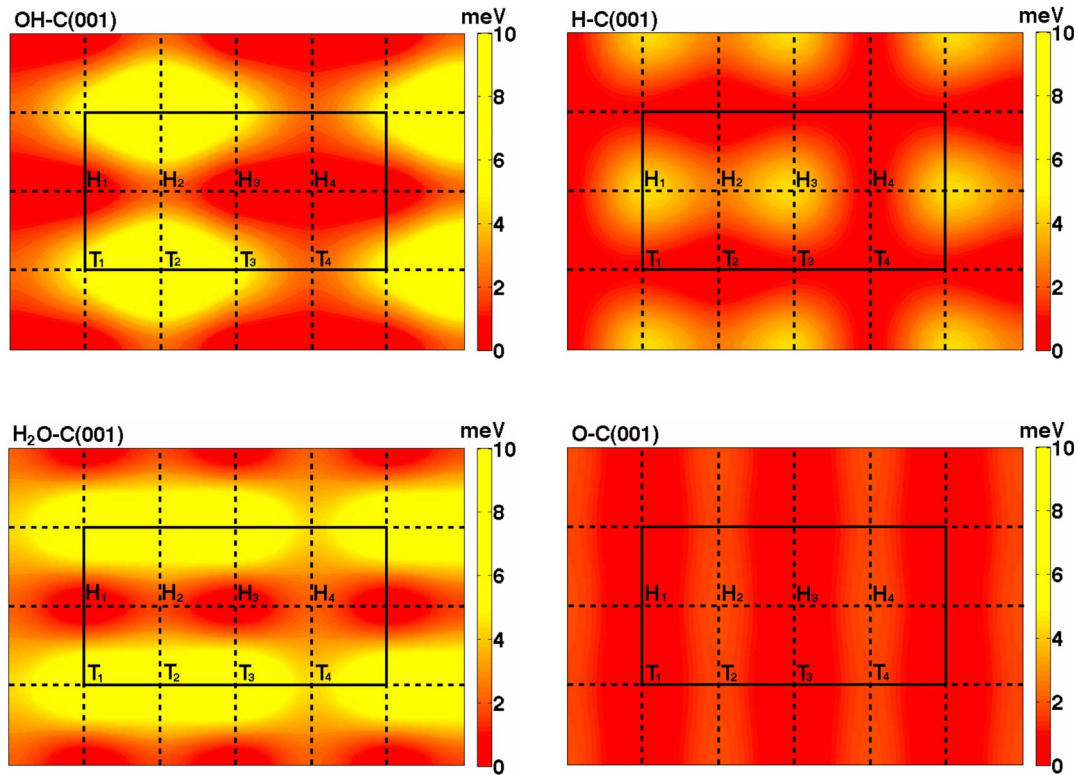
FIG. 7. (Color online) Lateral PESs calculated for the relative motion of commensurate surfaces presenting the same termination. The pictures are obtained by interpolating the values of the interaction energy at the eight grid points used to sample the (2×1) surface unit cell (Fig. 1). Different colors represent different values of the adhesion energy relative to its absolute minimum; they range from 0 to 10 meV. A common energy scale is used for all the bidimensional plots to allow to compare the corrugation and anisotropy of the four sliding interfaces.

apart because of the repulsive interaction between the partially ionized adsorbates. We remember that the oxygen atoms of the topmost layer of the O-C(001) surface possess an excess of $-0.3e$ negative charge. Furthermore, the small size of the adsorbates compared to hydroxyl groups makes the morphology of the hydrogenated and the oxygenated surfaces smoother than that of the hydroxylated surfaces. This is reflected in the features of the interface potential. As we can see from Figs. 7(a) and 7(b), the maxima of the PES of the OH-C(001) and H_2O interfaces are located at the lateral positions where the superposition of the OH groups is higher, corresponding, respectively, to the T_2 and T_3 grid points (last column of Table III). Thus the steric repulsion between the adsorbates causes the maxima of the PES of hydroxylated interfaces to become more pronounced compared to those in the hydrogenated and the oxygenated interfaces, leading to higher values of the potential corrugation.

The forces acting against the relative motion of two surfaces in a given direction can be obtained as the derivative of the potential along that direction. Thus, from the L-PES, one can derive the map of the friction forces intervening during the surface relative motion and evaluate the friction anisotropy. By looking at Fig. 7 we can expect an almost isotropic behavior of friction in hydrogenated and oxygenated interfaces, while the clear separation in energy between the hollow and the top sliding channels presented by the hydroxyl-containing interfaces should give rise to friction anisotropy. In particular, the highest resistance against sliding should be measured along the [100] and [$\bar{1}$10] directions for the OH-C(001) and H_2O-C(001) interfaces, respectively.

IV. CONCLUSIONS

A recent experiment demonstrates that the ultralow friction measured for diamond films in air originates because of the surface passivation occurring through the dissociative adsorption of the molecules contained in the gaseous atmosphere.[13] This finding, in agreement with previous experimental observations on the environmental effects on friction of diamond films or DLCs, demonstrates the link between the surface chemistry and the nanoscale friction. Motivated by these results, we performed an *ab initio* study based on DFT-GGA calculations on the properties of passivated diamond surfaces and interfaces. We considered the (2×1)-C(001) surface, taking into account the hydroxyl termination, the termination produced by the dissociative adsorption of one water molecule per unit cell, the hydrogen termination, and the oxygen termination. We identified the most stable geometry for each surface termination and we calculated the atomic charges. For all the terminations, we identified the presence of highly polarized bonds at the surface. We then evaluated the surface stability in different conditions, which account for the presence in the environment of H_2, O_2, and H_2O molecules in different concentrations, and we calculated surface phase diagram.

As a next step in our analysis, we considered interfaces obtained by facing two passivated surfaces. During the relaxation process the two slabs initially positioned at close distance repulse each other moving far apart until they reach an equilibrium distance which ranges from 2.5 Å for the interface containing both CH and OH bonds to 3.6 Å in the case of fully oxygenated interfaces. This behavior, together with the features of the P-PES obtained calculating the interface energy as a function of the surface separation, indicates that the complete saturation of the surface bonds and the existence of fractional charges on the adsorbates induce a high surface repulsion at short range. The small adhesion energy we calculated, which is of few meV per (2×1) cell, is determined by the long-range attraction between the surface dipoles. The adhesion energy we calculated between fully hydrogenated surfaces compares well with the experimental value reported for a diamond tip on an ultrananocristalline diamond surface after exposure to atomic hydrogen.

Finally, we calculated the variation in the adhesion energy as one surface translates along the underlying one, constructing the PES experienced by a sliding interface. All the PESs calculated for the different terminated interfaces presented a small corrugation (lower than 10 meV). The smoother PESs are those obtained for the hydrogenated and the oxygenated interfaces; the latter is almost flat. The presence of hydroxyl groups produces a slight increase in the PES corrugation and gives rise to a friction anisotropy.

---

*mcrighi@unimore.it

[1] D. S. Grierson and R. W. Carpick, Nanotoday **2** (5), 12 (2007).

[2] M. N. Gardos and S. A. Gabelich, Tribol. Lett. **6**, 87 (1999).

[3] M. N. Gardos and S. A. Gabelich, Tribol. Lett. **6**, 103 (1999).

[4] R. J. A. van den Oetelaar and C. F. J. Flipse, Surf. Sci. **384**, L828 (1997).

[5] A. Erdemir, Surf. Coat. Technol. **146–147**, 292 (2001).

[6] A. Erdemir and C. Donnet, J. Phys. D **39**, R311 (2006).

[7] A. V. Sumant, D. S. Grierson, J. E. Gerbi, J. A. Carlisle, O. Auciello, and R. W. Carpick, Phys. Rev. B **76**, 235429 (2007).

[8] S. Zhang, G. Wagner, S. N. Medyanik, W. K. Liu, Y. H. Yu, and Y. W. Chung, Surf. Coat. Technol. **177–178**, 818 (2004).

[9] G. T. Gao, P. T. Mikulski, G. M. Chateauneuf, and J. A. Harrison, J. Phys. Chem. B **107**, 11082 (2003).

[10] S. Dag and S. Ciraci, Phys. Rev. B **70**, 241401(R) (2004).

[11] A. Laikhtman, A. Lafosse, Y. Le Coat, R. Azria, and A. Hoffman, Surf. Sci. **551**, 99 (2004).

[12] X. Gao, L. Liu, D. Qi, S. Chen, A. T. S. Wee, T. Ouyang, K. P. Loh, X. Yu, and H. O. Moser, J. Phys. Chem. C **112**, 2487 (2008).

[13] A. R. Konicek, D. S. Grierson, P. U. Gilbert, W. G. Sawyer, A. V. Sumant, and R. W. Carpick, Phys. Rev. Lett. **100**, 235502 (2008).

[14] M. Kano, Y. Yasuda, Y. Okamoto, Y. Mabuchi, T. Hamada, T. Ueno, J. Ye, S. Konishi, S. Takeshima, J. M. Martin, M. I. De Barros Bouchet, and T. Le Mogne, Tribol. Lett. **18**, 245 (2005).

[15] L. Joly-Pottuz, C. Matta, M. I. de Barros Bouchet, B. Vacher, J. M. Martin, and T. Sagawa, J. Appl. Phys. **102**, 064912 (2007).

[16] H. Ronkainen, S. Varjus, and K. Holmberg, Wear **249**, 267 (2001).

[17] H. Ronkainen, S. Varjus, and K. Holmberg, Wear **222**, 120 (1998).

[18] B. Sun, X. Zhang, and Z. Lin, Phys. Rev. B **47**, 9816 (1993).

[19] A. Szabo and N. Ostlund, *Modern Quantum Chemistry* (Dover, New York, 1996).

[20] S. Baroni, A. Dal Corso, S. De Gironcoli, and P. Giannozzi, http://www.pwscf.org, 2001.

[21] J. P. Perdew, J. A. Chevary, S. H. Vosko, K. A. Jackson, M. R. Pederson, D. J. Singh, and C. Fiolhais, Phys. Rev. B **46**, 6671 (1992).

[22] J. P. Perdew, K. Burke, and M. Ernzerhof, Phys. Rev. Lett. **77**, 3865 (1996).

[23] *Zahlenwerte und Funktionen aus Naturwissenchaften una Technik*, edited by O. Madelung and M. Schulz, Landolt-Börnstein, New Series, Group III, Vol. 22, Pt. A (Springer-Verlag, Berlin, 1987).

[24] H. J. Monkhorst and J. D. Pack, Phys. Rev. B **13**, 5188 (1976).

[25] We tested different **k**-point sampling by calculating the energy of bulk diamond in an orthorhombic unit cell which was then replicated two times along the [110] direction and one time along the [$\bar{1}$10] to construct the slab with the (2×1) periodicity employed in surface calculations. In the latter calculations we used an equivalent **k**-point sampling to that identified of convergence for bulk energy. The total energy of the bulk unit cell, which contains four atoms, obtained with a 8×8 MP grid differs from that obtained with a 10×10 MP grid of 0.9 meV; while the energy difference obtained with the 10×10 grid and with a 12×12 grid is of 0.01 meV. We thus considered to have reached the convergence of total energy with a 10×10 MP grid.

[26] M. W. Chase, J. Phys. Chem. Ref. Data Monogr. **9**, 1 (1998).

[27] J. N. Israelachvili, *Intermolecular and Surface Forces* (Academic, New York, 1992).

[28] C. Kress, M. Fiedler, W. G. Schmidt, and F. Bechstedt, Phys. Rev. B **50**, 17697 (1994).

[29] Y. Okamoto, Phys. Rev. B **58**, 6760 (1998).

[30] Y. Qi, E. Konca, and A. T. Alpas, Surf. Sci. **600**, 2955 (2006).

[31] A. A. Stekolnikov, J. Furthmüller, and F. Bechstedt, Phys. Rev. B **65**, 115318 (2002).

[32] V. Chakrapani, J. C. Angus, A. B. Anderson, S. D. Wolter, B. R. Stoner, and G. U. Sumanasekera, Science **318**, 1424 (2007).

[33] G. Zilibotti, M. C. Righi, and M. Ferrario (unpublished).

[34] S. J. Sque, R. Jones, and P. R. Briddon, Phys. Rev. B **73**, 085313 (2006).

[35] M. J. Rutter and J. Robertson, Phys. Rev. B **57**, 9241 (1998).